Research Article

Coupled Thermomechanical Dynamics of Phase Transitions in Shape Memory Alloys and Related Nonlinear Phenomena

Korondo Rabaï[1], C. Adoukatl[1], E. Siryabe[2*], G.E. Ntamack[1], S. Charif D'Ouazzane[3]

[1]Groupe de Mécanique, Matériaux et Acoustique (GMMA), Département de physique, Faculté des Sciences, Université de Ngaoundéré BP. 454, Cameroun
[2]Groupe Evaluation Non Destructive, Safran Helicopter Engines, Avenue Joseph Szydlowski, 64510 Bordes, France
[3]Laboratoire de Mécanique, Thermique et Matériaux (LMTM), École Nationale de l'Industrie Minérale, B.P. 753 Rabat, Maroc
 E-mail: esiryabe@yahoo.fr

Abstract: The aim of this paper is to study the coupled non-linear dynamics of the behaviour of Shape Memory Alloys (SMA) under harmonic excitation. The thermomechanical model developed by Falk and based on Landau theory is used to describe the coupled thermomechanical behaviour of the SMA mass-damper-bar system. Fully coupled mechanical and thermal field equations are established to reveal the strong coupling phenomena arising from the phase transition. Then, the harmonic balance method is used to obtain the steady-state frequency responses. The effect of thermomechanical coupling on the frequency and time response curves is taken into account by modifying the heat transfer coefficient. The results show that deformation and temperature provide a stable sinusoidal response. The analysis of the results leads to different ways of controlling the nature and extent of the coupled and non-linear response of SMA-based oscillators. Comparison of the analytical results with experimental data from the literature validates the coupled thermomechanical nonlinear model. These results can be used effectively to control the external vibrations of various systems.

Keywords: shape memory alloy; mass-bar-damper system; thermomechanical coupling; martensitic transformation and hysteresis loops

1. Introduction

Nowadays, one of the most essential elements of structural design for civil engineers is to build a system that is adaptable to environmental conditions. In this context, technological innovation and scientific advances in the field of novel materials with strong multiphysical coupling have led to the development of so-called smart and adaptive materials [1]. This class of materials, typically used as sensors and actuators, has the ability to change its shape and stiffness by the imposition of electric, electromagnetic, thermal or stress fields [1]. Shape memory alloy (SMA) are a class of smart materials with remarkable thermomechanical properties such as shape memory effect and pseudoelasticity [2]. These properties result from the phenomenon of phase transition between austenite and martensite at different stress and temperature conditions. Due to this behaviour, SMAs are used in vibration control, noise reduction [3], in actuation system and in vibration isolation system [4]. The pseudo-elastic nature of the phase transformation makes them very good candidates for vibration damping devices [5]. However, the inherent non-linearity and strong thermo-mechanical coupling observed in the behaviour of SMAs during phase transitions makes modelling difficult for most applications. Several research has been undertaken on the modelling

and application of SMAs in structural systems to support applied dynamic loads in the form of vibration control systems.

For example, based on the model developed by Morin et *al.*[6], Moussa et *al.*[7] have numerically studied the forced responses of an oscillator reproducing the pseudo-elastic behaviour of SMA. The time integration of the equations of motion with the reduced model was performed using a Newmark scheme. Non-linear features of the damper response were observed, including jumps, period doubling, symmetry breaking bifurcations and chaotic responses. However, the study does not take into account the energy dissipation during the phase transition, which results in hysteresis loops. Oliveira et *al.*[8] numerically studied the dynamic jumps in a shape memory oscillator whose stiffness is described by the Fremond model [9]. The fourth-order Runge-Kutta numerical method is used to solve the constitutive equations of the system. The numerical simulation results have dynamic jumps as a consequence of abrupt changes in the SMA system behaviour during the phase transition appear in the frequency responses of the system. However, the model makes solving the problem complex due to several internal variables. Enemark et *al.*[10] performed experimental and theoretical analysis of a one-degree-of-freedom oscillator with a pseudo-elastic SMA element. They showed that the system has a complex non-linear behaviour due to the complex thermo-mechanical relationships of the pseudo-elastic SMA spring. Their study were able to predict the overall non-linear behaviour of the system. Gaikward et *al.*[11] also performed nonlinear dynamic analysis of shape memory devices with Duffing and Quadratic oscillators using the harmonic equilibrium method and the averaging method to find near-resonant responses. They showed that the strength of change due to the quadratic non-linearity is less than that due to the cubic non-linearity. It was observed that the SMA-based oscillator not only reduces the displacement amplitude effectively, but can also be used to tune the nature of the nonlinearity from softening to hardening.

To consider both non-linearity and hysteresis, Zhuo et *al.*[12] studied the responses of a bar in SMA by developing the piecewise linear hysteretic model to reproduce the pseudo-elastic behaviour of NiTi SMAs. They showed that the softening non-linearity induced by the phase transition bends the frequency response curve to the left, while the subsequent martensite hardening further bends the frequency response curve to the right, leading to multi-valued regions and jump phenomena. Hysteresis has the effect of suppressing the amplitude of the system response. However, their model ignores the influence of temperature. In order to take into account non-linearity and temperature, the authors [13–15] simultaneously studied the influence of non-linearity and temperature on the responses of a shape memory oscillator by developing a polynomial model to describe the stiffness. They showed that at low temperatures, the force-strain relationship is strongly non-linear and the system has a smoothing behaviour. Whereas at high temperatures the force-strain relationship becomes linear and the material displays a hardening behaviour. However, their study was carried out under isothermal loading conditions. Studies under dynamic loading of the thermomechanical coupled SMA oscillator have been also studied in the literature [16–19]. Most of them use numerical or experimental methods and do not explicitly distinguish the effects of non-linearity and thermomechanical coupling. In contrast, the combination of analytical solutions and numerical results can overcome these difficulties.

In vibratory systems containing SMA bar, the restoring force is non-linear and thermomechanically coupled due to the phenomenon of phase transitions. SMA Type NiTi with a composition of 55.4 wt% Ni is used. This type of alloy known under the trade name Nitinol (Nickel Titanium Naval Ordnance Laboratory) is superelastic at room temperature 25°C [20]. A polynomial model, based on Landau's theory and proposed by Falk [21] is used to describe the behaviour of SMAs. The model has the following expression:

$$\psi\left(\varepsilon,T\right) = \frac{k_1\left(T-T_M\right)}{2}\varepsilon^2 - \frac{k_2}{4}\varepsilon^4 + \frac{k_3}{6}\varepsilon^6 \tag{1}$$

where k_1, k_2, k_2 are related to the second, third, and fourth order elastic constants, respectively [22]. ε the strain field, T the temperature field, T_M is the temperature below which the martensite phase is stable.

As shown in

Figure 1(a), the minimum and maximum points represent the stability and instability of each phase of the SMA. Where M+ and M- are the two stable variants of the martensite phase induced by tension and compression respectively, A the austenite phase of SMA and T_A the temperature above which the austenite phase is stable [23]. T_A is expressed as:

$$T_A = T_M + \frac{k_2^2}{4k_1k_3} \tag{2}$$

The stress dependence σ is based on Landau's theory of a polynomial-free energy ψ, which was initially proposed in [24]:

$$\sigma(\varepsilon, T) = \frac{\partial \psi(\varepsilon, T)}{\partial \varepsilon} = k_1(T - T_M)\varepsilon - k_2\varepsilon^3 + k_3\varepsilon^5 \tag{3}$$

The stress-strain curve derived from the polynomial model is presented in

Figure 1(b). It shows that at a relatively low temperature, the SMA has a shape memory behaviour. While when the temperature is relatively high, the SMAs display a pseudo-elastic behaviour [25].

(a)   (b)
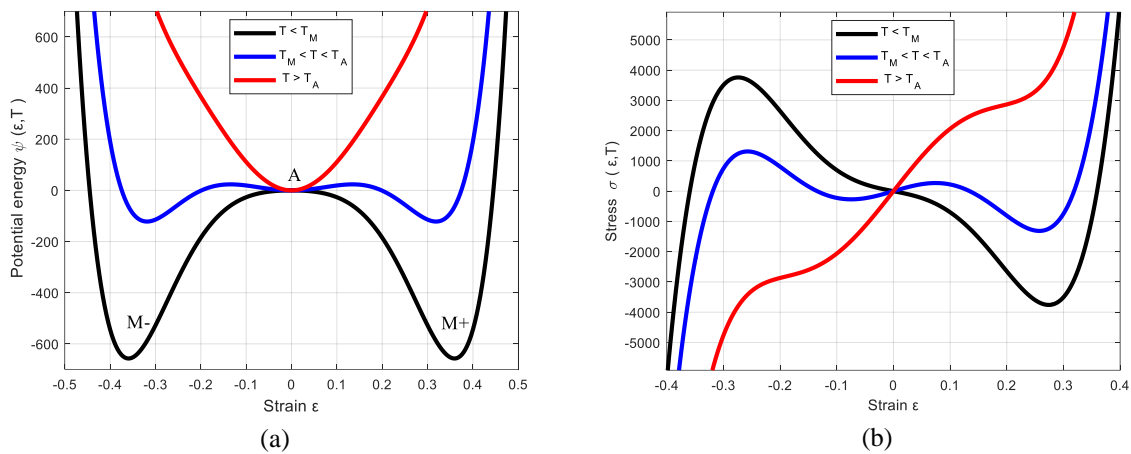
Figure 1. (a) Potential energy curve and (b) Stress-strain at different temperatures

In this study, we present the mechanical and thermal responses of a non-linear vibration control device containing an NiTi SMA bar through a shape memory oscillator. An SMA bar is applied in the vibration system as a spring element providing the restoring force. Due to the phase transitions in SMA, the restoring force is non-linear and thermomechanically coupled. To consider the non-linearity and thermo-mechanical coupling, le polynomial model, based on Landau theory is used to describe the behaviour of SMA bar. The harmonic balance method and the fourth-order Runge-Kutta numerical method are then used to solve the equation of motion of the system. The analytical approach allows us to find steady-state frequency responses. Based on the analytical results, we draw frequency response curves (FRC) to show the influence of heat transfer times at different environmental temperatures. The obtained FRC are compared with FRC in the literature. As for the numerical approach, it allows us to find responses in the time domain and thus reveal the hysteresis loop phenomenon due to thermomechanical coupling. Finally, numerical results are compared to the experimental data obtained in the literature.

2. Shape memory oscillator model

To study the dynamic behavior of SMAs, we will consider a one-degree-of-freedom oscillator consisting of a mass m, connected to a rigid support *via* a viscous damping coefficient ν and an SMA bar. Damping is due to the movement of interphases between the different phases [26]. On a macroscopic scale, it reflects the viscous effects of phase transformation [27]. The SMA bar are considered as nonlinear spring as shown in

Figure 2. In a dynamical system containing SMAs, the nonlinear stiffness and the damping capacity arise from the nature of the phase transition and manifest themselves macroscopically through the stress-strain-temperature relationship. Stiffness and damping capacity can be influenced by thermomechanical coupling. For simplicity, the softening stiffness and the hysteresis loop of the stress-strain-temperature relationship of the SMA bar are modeled separately as a nonlinear spring and a viscous damper in the theoretical analysis (

Figure 2). During the phase transition, the stiffness of the SMA bar varies non-monotonically with strain and temperature. Thus, it is related to internal stress $\sigma(\varepsilon, T)$ by the following relation [28]:

$$F_R(\varepsilon, T) = A.\sigma(\varepsilon, T) \tag{4}$$

where A is the cross section of the SMA bar.
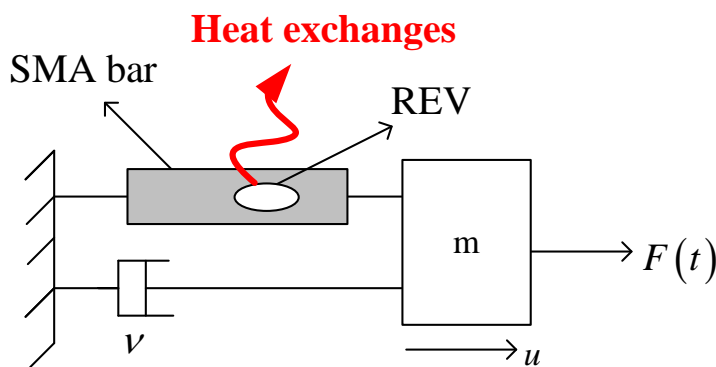
Figure 2. Model of the shape memory oscillator [6]

2.1 *Thermomechanical coupled equation of the system*

The thermomechanical-coupled equation includes the equation of motion and the equation of heat.

2.1.1 Equation of motion

The dynamic equation of the non-linear mass-spring oscillator (

Figure 2) with harmonic $F(t)$ has the following expression [15]:

$$m\frac{d^2u}{dt^2} + v\frac{d\varepsilon}{dt} + F_R(\varepsilon, T) = F(t) \tag{5}$$

where u is the mass displacement m, v is the viscous damping coefficient, $F(t) = F_0\cos(\omega t)$ is the external excitation and $F_R(\varepsilon, T)$ is the restoring force provided by the SMA bar.

The vibration being longitudinal, the displacement u of the mass is linked to the deformation field ε developed within the SMA bar by relation [29]:

$$u = L\varepsilon \tag{6}$$

where L is the length of the bar.

Substitution of equations (4) and (6) in equation (5) and after manipulation we obtain the reduced form of the mechanical equation:

$$\ddot{\varepsilon}(t) + 2\zeta\dot{\varepsilon}(t) + \alpha(T(t) - T_M)\varepsilon(t) + \beta\varepsilon^3(t) + \gamma\varepsilon^5(t) = f_0\cos(\omega t) \tag{7}$$

With $\qquad \ddot{\varepsilon} = \dfrac{d^2\varepsilon}{dt^2}; \dot{\varepsilon} = \dfrac{d\varepsilon}{dt}; \zeta = \dfrac{v}{2mL}; \alpha = \dfrac{Ak_1}{mL}; \beta = \dfrac{Ak_2}{mL}; \gamma = \dfrac{Ak_3}{mL}; f_0 = \dfrac{F_0}{mL}$

2.1.2 Heat equation

The method for constructing the equation of motion or evolution for the mean volume temperature $T(t)$ of the bar is essentially based on the heat transfer equation and global analysis [30]. It is well known that for a body of volume V and boundary surface S (Figure 3), the differential heat transfer equation can be derived from the local energy balance at any position x , as:

$$\lambda\frac{\partial T(\mathrm{x},t)}{\partial t} - \nabla.q(\mathrm{x},t) = g(\mathrm{x},t) \tag{8}$$

where $\lambda = \rho c$ is the heat capacity per unit volume, ρ density, c specific heat capacity per unit mass q is the heat flux and $g(\mathrm{x},t)$ is the heat source.
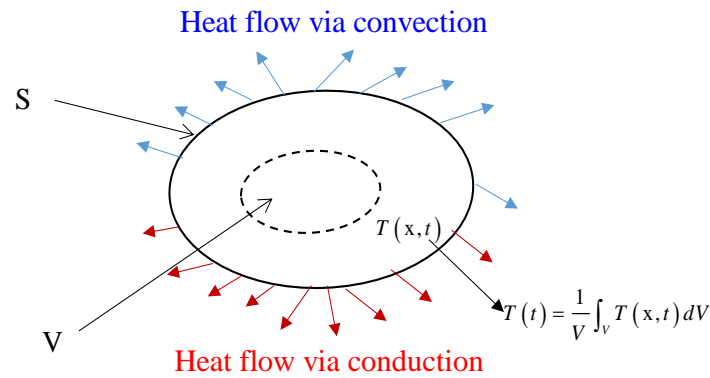
Figure 3. Schematic diagram of heat transfer through the representative elemental volume (REV) [31]

The lumped system analysis can be applied to equation (8) for the body under low temperature gradient conditions and can give a very simplified expression of the volume mean temperature. An average global volume of equation (8) in the region V not only defines the volume average temperature $T(t) = \frac{1}{V}\int_V T(\mathrm{x},t)\,dV$ which is a function of time only, but also transforms equation (8) as:

$$\lambda\frac{\partial T(t)}{\partial t} - \frac{1}{V}\int_V \nabla.\mathrm{q}(\mathrm{x},t)\,dV = g(t), \qquad\qquad x \in V, t > 0 \qquad (9)$$

where $g(t) = \frac{1}{V}\int_V g(\mathrm{x},t)\,dV$

We now derive the evolution of the volume mean temperature of the sample $T(t)$ by localized system analysis. To simplify the step, we used the following assumptions:

(i). Latent heat release/absorption and hysteresis heat release are the two internal heat sources of the material and their rates are approximated as being proportional to the applied strain rate and the square of the strain rate respectively, without separating the loading-unloading process in different subsections [32].

(ii). The heat flow through the two handles is modeled as heat conduction through the two end cross sections of the gauge, which undergoes a cyclic phase transition.

The heat source $g(t)$ in equation (9) includes the latent heat l_0 and the hysteresis heat D. The latent heat arises from the phase transition and hence the rate of latent heat release can be assumed proportional to the rate of strain. Taking into account the assumption (i), we can write the latent heat release rate in the form $l_0\frac{\omega}{2}\sin(\omega t)$ that satisfies the condition that the integral of the latent heat release rate during loading and unloading is l_0 and $-l_0$ respectively. At the same time, friction-like hysteresis heat is released and its rate increases with strain rate, is always positive in both load and unload conditions. We therefore simply assume that the hysteresis heat release rate is proportional to the square of the strain rate in the form $D\frac{\omega}{\pi}\sin^2(\omega t)$. The assumption we made is mainly to simplify the model and ensure that hysteresis heat release is always positive during loading and unloading. We also ensure that the total hysteresis heat released in a cycle is D.

Thus, the average heat source in volume $g(t)$ is written as follow:

$$g(t) = \frac{1}{V}\int_V g(x,t)\,dV = \frac{l_0\omega}{2}\sin(\omega t) + \frac{D\omega}{\pi}\sin^2(\omega t) \qquad (10)$$

Applying the law of divergence, the volume integral of the local term is the outward heat exchange with the ambient and assuming that the temperature is uniform in the bar [19]:

$$\int_V \nabla.\mathrm{q}\,dV = \int_S \mathrm{q}.\mathrm{n}\,dS = hA(T - T_0) \qquad (11)$$

where n is the unit normal vector pointing outwards to the surface of the volume, h is the convective heat transfer coefficient, A is the cross section of the SMA bar and T_0 the temperature of the surrounding medium.

By substituting equations (10) and (11) in equation (9) the heat equation through the REV is written as:

$$\dot{T}(t) = -\frac{1}{t_h}\left(T(t) - T_0\right) + \frac{l_0\omega}{2\lambda}\sin\left(\omega t\right) + \frac{D\omega}{\pi\lambda}\sin^2\left(\omega t\right) \tag{12}$$

where $\dot{T} = \dfrac{\partial T(t)}{\partial t}$, $t_h = \dfrac{\lambda V}{hA}$ convective heat transfer time, h is the natural convection coefficient of the side surface in the air and depends on the temperature difference and D is the dissipation of mechanical energy per unit volume of the nth cycle [33].

The hysteresis loop area D in the steady-state cycle can be easily obtained using the steady-state temperature [20]:

$$D = \frac{D_0 + \dfrac{\left(k_f + k_r\right)\pi l_0 t_h \omega \varepsilon_{max}}{8\lambda\left(1 + \omega^2 t_h^2\right)}}{1 + \dfrac{\left(k_f - k_r\right)t_h \omega \varepsilon_{max}}{2\pi\lambda}} \tag{13}$$

Finally, the constitutive equations describing the evolution of the coupled thermomechanical behavior of the shape memory oscillator are obtained by combining the equations (7) and (12):

$$\begin{cases} \ddot{\varepsilon}(t) + 2\zeta\dot{\varepsilon}(t) + f_R\left(\varepsilon(t), T(t)\right) = f_0\cos\left(\omega t\right) \\ \dot{T}(t) = -\frac{1}{t_h}\left(T(t) - T_0\right) + \frac{D\omega}{2\pi\lambda} + \frac{l_0\omega}{2\lambda}\sin\left(\omega t\right) - \frac{D\omega}{2\pi\lambda}\cos\left(2\omega T\right) \end{cases} \tag{14}$$

with

$$f_R\left(\varepsilon(t), T(t)\right) = \alpha\left(T(t) - T_M\right)\varepsilon(t) + \beta\varepsilon^3(t) + \gamma\varepsilon^5(t) \tag{15}$$

2.2 Resolution of the equations

As the response of an SMA vibration system usually first experience a transient state and eventually reaches a steady state, in this section, the first-order harmonic balance method and the fourth-order Runge-Kutta method are used to obtain expressions of steady-state and transient responses.

2.2.1 Steady state solution

In the case of vibrations with periodic external stresses, the main assumption consists in assuming that the response of a nonlinear system to a periodic excitation is a sinusoidal function of time with the same frequency as the excitation. Although it is unlikely that there is an explicit analytical solution for such a nonlinear-coupled vibrational system, an approximate analytical approach can be used to obtain the steady-state responses and reveal the roles of nonlinearity and thermomechanical coupling. With this hypothesis, the answers $\varepsilon(t)$ and $T(t)$ can be developed into Fourier series [34] as:

$$\begin{cases} \varepsilon(t) = a_0 + \sum_{n=1}^{N} a_n\cos\left(n\omega t\right) + b_n\sin\left(n\omega t\right) \\ T(t) = A_0 + \sum_{n=1}^{N} A_n\cos\left(n\omega t\right) + B_n\sin\left(n\omega t\right) \end{cases} \tag{16}$$

where a_0, a_1, b_1 and A_0, A_1, B_1 are the coefficients of the associated harmonic functions and N is the highest order of the harmonics considered.

In the same way, the nonlinear forces are written in the form of Fourier series:

$$f_R\left(\varepsilon\left(t\right),T\left(t\right)\right)=f_{c0}+\sum_{n=1}^{N}f_{cn}\cos\left(n\omega t\right)+f_{sn}\sin\left(n\omega t\right) \tag{17}$$

The residues are defined in the time domain as follows:

$$\begin{cases} R_1\left(t\right)=\ddot{\varepsilon}\left(t\right)+2\zeta\dot{\varepsilon}\left(t\right)+f_R\left(\varepsilon\left(t\right),T\left(t\right)\right)-f_0\cos\left(\omega t\right) \\ R_2\left(t\right)=\dot{T}\left(t\right)+\dfrac{1}{t_h}\left(T\left(t\right)-T_0\right)-\dfrac{D\omega}{2\lambda\pi}-\dfrac{l_0\omega}{2\lambda}\sin\left(\omega t\right)+\dfrac{D\omega}{2\lambda\pi}\cos\left(2\omega t\right) \end{cases} \tag{18}$$

To solve equation (18) , we use the Galerkin procedure which consists in calculating the average over a period $\tau=\dfrac{2\pi}{\omega}$ of the residual functions $R_1\left(t\right)$ and $R_2\left(t\right)$ *via* the properties of the basic $\cos\left(n\omega t\right)$ and $\sin\left(n\omega t\right)$ following functions:

$$\begin{cases} \dfrac{2}{\tau}\displaystyle\int_0^{\tau}\cos\left(i\omega t\right)\cos\left(j\omega t\right)dt=\delta_{ij} \\[2mm] \dfrac{2}{\tau}\displaystyle\int_0^{\tau}\sin\left(i\omega t\right)\sin\left(j\omega t\right)dt=\delta_{ij} \\[2mm] \dfrac{2}{\tau}\displaystyle\int_0^{\tau}\sin\left(i\omega t\right)\cos\left(j\omega t\right)dt=0 \end{cases} \tag{19}$$

where $\delta_{ij}=\begin{cases} 1,i=j \\ 0,i\neq j \end{cases}$

The projection of each of these residual functions onto each base function gives us:

$$N=0,\qquad \begin{cases} \dfrac{2}{\tau}\displaystyle\int_0^{\tau}R_1\left(X_0,t\right)dt=0 \\[2mm] \dfrac{2}{\tau}\displaystyle\int_0^{\tau}R_2\left(X_0,t\right)dt=0 \end{cases} \Rightarrow \begin{cases} f_{c0}=0 \\[2mm] A_0-T_0-\dfrac{D\omega t_h}{2\lambda\pi}=0 \end{cases} \tag{20}$$

$$N=1,\qquad \begin{cases} \begin{cases} \dfrac{2}{\tau}\displaystyle\int_0^{\tau}R_1\left(t\right).\cos\left(\omega t\right)dt=0 \\[2mm] \dfrac{2}{\tau}\displaystyle\int_0^{\tau}R_1\left(t\right).\sin\left(\omega t\right)dt=0 \end{cases} \Rightarrow \begin{cases} -\omega^2a_1+2\zeta\omega b_1+f_{c1}-f_0=0 \\[2mm] -2\zeta\omega a_1-\omega^2b_1+f_{s1}=0 \end{cases} \\[8mm] \begin{cases} \dfrac{2}{\tau}\displaystyle\int_0^{\tau}R_2\left(t\right).\cos\left(\omega t\right)dt=0 \\[2mm] \dfrac{2}{\tau}\displaystyle\int_0^{\tau}R_2\left(t\right).\sin\left(\omega t\right)dt=0 \end{cases} \Rightarrow \begin{cases} \omega t_hB_1+A_1=0 \\[2mm] -\omega t_hA_1+B_1=\dfrac{l_0\omega t_h}{2\lambda} \end{cases} \end{cases} \tag{21}$$

with

$$\begin{cases} f_{c0}=\dfrac{2}{\tau}\displaystyle\int_0^{\tau}f_R\left(\varepsilon,t\right)dt \\[2mm] f_{c1}=\dfrac{2}{\tau}\displaystyle\int_0^{\tau}f_R\left(\varepsilon,t\right)\cos\left(\omega t\right)dt \\[2mm] f_{s1}=\dfrac{2}{\tau}\displaystyle\int_0^{\tau}f_R\left(\varepsilon,t\right)\sin\left(\omega t\right)dt \end{cases} \tag{22}$$

Referring to equation (15), we calculate f_{c0},f_{c1} and f_{s1} and obtain the following expressions:

$$f_{c0} = \frac{\alpha}{2}\left(2a_0\left(A_0 - T_M\right) + b_1 B_1\right) + \frac{\beta}{2}a_0\left(2a_0^2 + 3\left(a_1^2 + b_1^2\right)\right) + \frac{\gamma}{4}a_0\left(8a_0^4 + 40a_0^2\left(a_1^2 + b_1^2\right) + 15\left(a_1^2 + b_1^2\right)^2\right)$$

$$f_{c1}\left(a_1, b_1\right) = \alpha\left(a_0 A_1 + a_1\left(A_0 - T_M\right)\right) + \frac{3\beta}{4}a_1\left(4a_0^2 + a_1^2 + b_1^2\right) + \frac{5\gamma}{8}a_1\left(8a_0^4 + 12a_0^2\left(a_1^2 + b_1^2\right) + \left(a_1^2 + b_1^2\right)^2\right) \quad (23)$$

$$f_{s1}\left(a_1, b_1\right) = \alpha\left(a_0 B_1 + b_1\left(A_0 - T_M\right)\right) + \frac{3\beta}{4}b_1\left(4a_0^2 + a_1^2 + b_1^2\right) + \frac{5\gamma}{8}b_1\left(8a_0^4 + 12a_0^2\left(a_1^2 + b_1^2\right) + \left(a_1^2 + b_1^2\right)^2\right)$$

By substituting equation (23) into equations (20) and (21), the mechanical $\varepsilon_1 = \left(a_1^2 + b_1^2\right)^{1/2}$ and thermal responses $T_1 = \left(A_1^2 + B_1^2\right)^{1/2}$ equations at the excitation frequency ω are obtained:

$$\begin{cases} \left(A^2 + \left(2\zeta\omega\right)^2\right)\varepsilon_1^2 - f_0^2 - \alpha a_0\left(\alpha a_0 T_1^2 - 2A_1 f_0\right) = 0 \\ 4\lambda^2\left(\omega^2 t_h^2 + 1\right)T_1^2 - l_0^2\omega^2 t_h^2 = 0 \end{cases} \quad (24)$$

where $A = -\omega^2 + \alpha\left(A_0 - T_M\right) + \frac{3}{4}\beta\varepsilon_1^2 + \frac{5}{8}\gamma\varepsilon_1^4 + \left(\frac{15}{2}\gamma\varepsilon_1^2 + 3\beta\right)a_0^2 + 5\gamma a_0^4$

In the following, the equations (24) are used to obtain the mechanical and thermal response curves in the frequency domain.

For the isothermal case of the thermomechanical model, the heat equation is ignored and the temperature is maintained at room temperature T_0. Of course, we can also leave h a large number $\left(h \to \infty \Rightarrow t_h \to 0\right)$ for the temperature to be calculated as nearly constant due to strong heat exchange. In this case if $a_0 = 0$ i.e. the oscillations take place around the static equilibrium point $\varepsilon = 0$ [35], we obtain the same expression obtained by Du et al.[15]:

$$\left(\left(\alpha\left(T_0 - T_M\right) - \omega^2\right)\varepsilon_1 + \frac{3\beta}{4}\varepsilon_1^3 + \frac{5\gamma}{8}\varepsilon_1^5\right)^2 + \left(2\zeta\omega\varepsilon_1\right)^2 = f_0^2 \quad (25)$$

2.1.2 Runge-Kutta method

The system of equation (14) can be solved numerically by the four-order Runge-Kutta method [36] as:

$$\begin{cases} \dfrac{dy}{dt} = f\left(t, y\right) \\ y\left(t_0\right) = y_0 \end{cases} \quad (26)$$

with $y = \begin{pmatrix} \varepsilon \\ v \\ T \end{pmatrix}$; $f\left(t, y\right) = \begin{pmatrix} v \\ -2\zeta v + f_R\left(\varepsilon, T\right) + f_0 \cos\left(\omega t\right) \\ -\dfrac{1}{t_h}\left(T - T_0\right) + \dfrac{l_0\omega}{2\lambda}\sin\left(\omega t\right) + \dfrac{D\omega}{\pi\lambda}\sin^2\left(\omega t\right) \end{pmatrix}$, $y_0 = \begin{pmatrix} \varepsilon_0 \\ v_0 \\ T_0 \end{pmatrix}$.

Where ε_0, v_0, T_0 are the initial values of ε, v, T respectively at $t = t_0$.

Assuming that the solution of the typical initial value problem (26) is $y = y\left(t\right)$, its Taylor expansion is written as:

$$y\left(t_{i+1}\right) = y\left(t_i\right) + \sum_{k=1}^{n} \frac{h^k}{k!}y^k\left(t_i\right) + 0 \quad (27)$$

Runge-Kutta method is essentially a numerical method indirectly using Taylor series. For the difference $\dfrac{y\left(t_{i+1}\right) - y\left(t_i\right)}{h}$, according to differential mean value theorem, $\exists \theta \in \left(0,1\right)$ satisfying:

$$\frac{y(t_{i+1}) - y(t_i)}{h} = y'(t + \theta h) \tag{28}$$

Therefore $y(t_{i+1}) = y(t_i) + hf(t_i + \theta h, y(t_i + \theta h))$.

Defining $K^* = f(t_i + \theta h, y(t_i + \theta h))$ as the average gradient in $[t_{i+1}, t_i]$, the K^* in the fourth-order Runge- Kutta method can therefore be calculated from the following expressions:

$$y_{i+1} = y_i + \frac{h}{6}(K_1 + 2K_2 + 2K_3 + K_4) \tag{29}$$

with :

$$h = t_{i+1} - t_i; K_1 = f(t_n, y_n); K_2 = f\left(t_n + \frac{h}{2}, y_n + \frac{h}{2}K_1\right); K_3 = f\left(t_n + \frac{h}{2}, y_n + \frac{h}{2}K_2\right); K_4 = f(t_n + h, y_n + hK_3)$$

3. Results and discussions

This section presents the frequency response curves (FRC) from the analytical solution, the hysteresis loop phenomenon and the time domain response curves; and discusses the effect of temperature and convective heat transfer time. The chemical, mechanical and thermal properties of the material are listed in the Table 1.

Table 1. Chemical, mechanical and thermal properties of the NiTi SMA [15, 20]

Properties	symbols	Units	Values
The specific heat capacity	c_p	J/ kgK	500
Volumic mass	ρ	kg /m^3	6450
Heat capacity per unit volume	$\lambda = \rho c_p$	J/m^{3}K	3.225×10^6
Latent heat	l_0	J/m^3	77.4×10^7
Overall convection coefficient	h	W /m^{2}K	100
Isothermal hysteresis loop zone	D_0	MPa	5.33
Temperature coefficient for forward transformation stress	k_f	MPa/K	6.56
Temperature coefficient for reverse transformation stress	k_r	MPa/K	7.09
Martensitic phase temperature	T_M	K	208
Ambient temperature	T_0	K	298
Viscous damping coefficient	v	Ns	100
Mass	m	Kg	5
Length	L	m	1

Amplitude of Excitation Force	F_0	N	2000
cross section	A	m^2	3.83×10^{-3}
Materials constants	k_1	$Kg / s^2 K$	459.6
	k_2	$Kg / s^2 m^2$	3.59×10^5
	k_3	$Kg / s^2 m^4$	3×10^6

3.1 *Hysteresis loops*

The hysteresis phenomenon translates the energy dissipation capacity of material when it passes from one phase to another. Although the phenomenon of hysteresis has been the subject of several studies in the literature [22, 39–41], here we represent this phenomenon from the semi-analytical expressions obtained by the Runge-Kutta method (equation (29)). The Figure 4 shows the thermal hysteresis. It is caused by the cooling and heating processes during heat exchange between material samples (conductive heat transfer) and between the material and the external environment (heat transfer by convection). The heating process induces a transformation M+ (Martensite) →A (Austenite), and another sharp jump in strain values occurs when the transformation takes place. The two sudden jumps in stress during the cooling A→M (upward arrow) and heating M → A (downward arrow) processes do not coincide (Figure 4(a)). In other words, the temperatures at which the transformations take place during the cooling and heating processes are different. Therefore, there is a hysteresis loop caused by the thermal load. The fact that the thermal hysteresis loop curves bend to the left and to the right is due to the softening non-linearity of the material behavior at high heat exchange (Figure 4 (a and b)) and the hardening non-linearity at low heat exchange (Figure 4(c)) respectively.

(a)

(b)
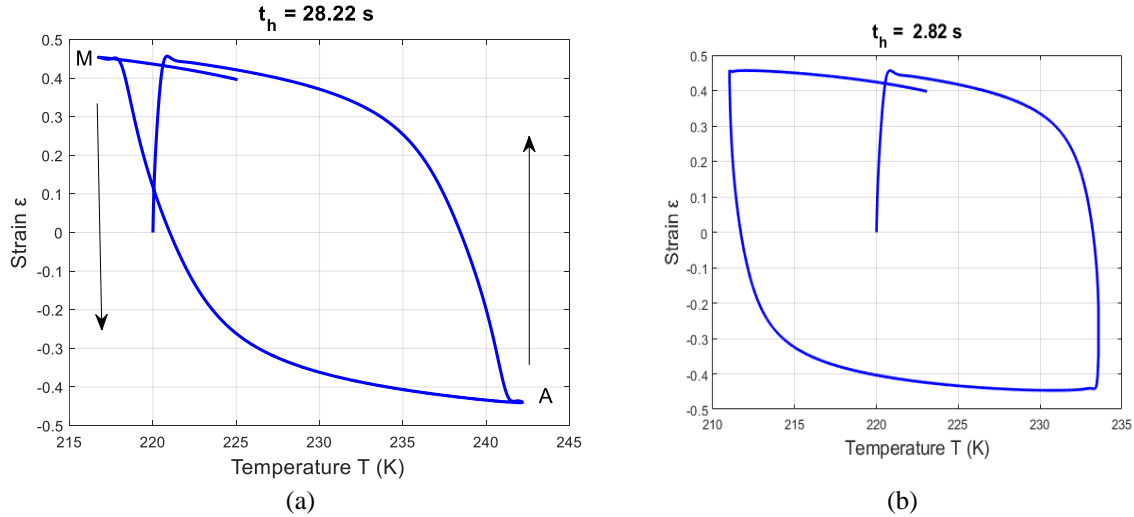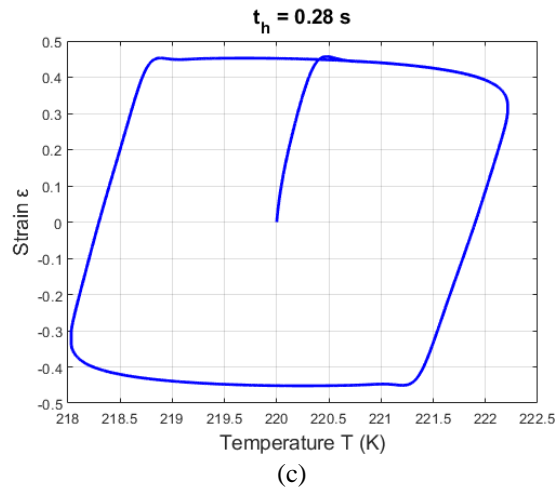
Figure 4. Thermal hysteresis loops at different heat transfer times

In order to validate the ability of the model to simulate the strain-temperature hysteresis of phase transitions in SMAs, the model predictions (with t_h=28.22s) are compared with the experimental data reported by Maletta et al.[40] (with t_h=30s). The

Figure 5 highlights the effect of the heat transfer time on the hysteresis loop. It shows that when the heat transfer time is large, the analytical result approaches the result of experimental data. Because the experiment was conducted under conditions of strong heat exchange. As the heat transfer time decreases, the hysteresis loop tends to disappear and the strain-temperature relationship tends to be linear. The two sudden jumps in strain during cooling processes A (austenite) →M (martensite) indicated by up arrow and heating processes M → A indicated by down arrow do not coincide [41] .The model prediction results are in good agreement with the experimental data. Thus, the developed model can be used in the following to analyse the influence of heat transfer on properties of SMA.
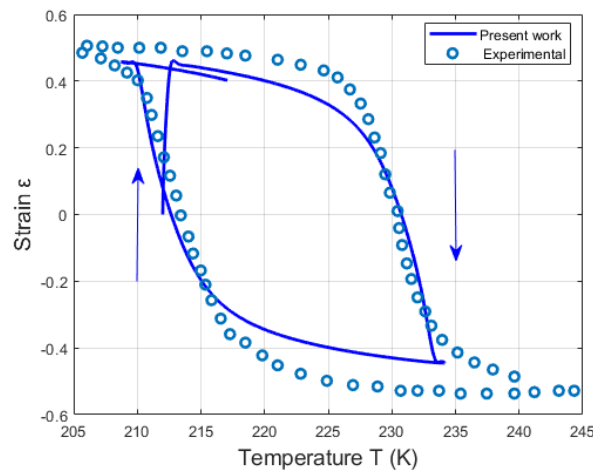
Figure 5. Comparisons between model predictions and experimental data reported by [40]

3.2 *Time domain analysis*

The influence of heat transfer time on the time responses is now investigated. It is found that at a large value of heat transfer time, the maximum amplitude of thermal response decreases with time (Figure 6). This decrease with time is due to the damping caused by the heat exchange of the material with the external environment. While at low values of heat transfer time, the thermal response evolves sinusoidally with time as in the undamped system. This shows that the SMA vibration system can go from a transient state to a permanent state. These time response curves are similar to those obtained by Yin et al.[20]. For the mechanical responses (Figure 7), the time of heat transfer has almost no influence. This is because the phase transition from martensite to austenite is induced by the temperature.
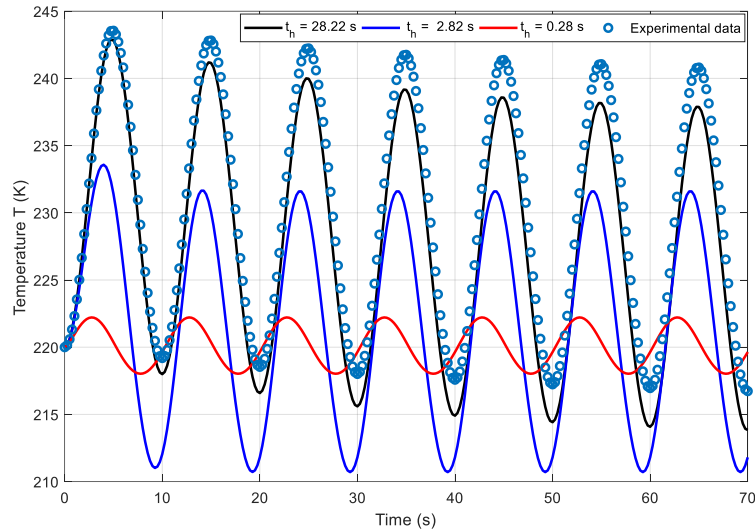
Figure 6. Temperature evolution curve as a function of heat transfer time, for an intermediate frequency 0.1 Hz
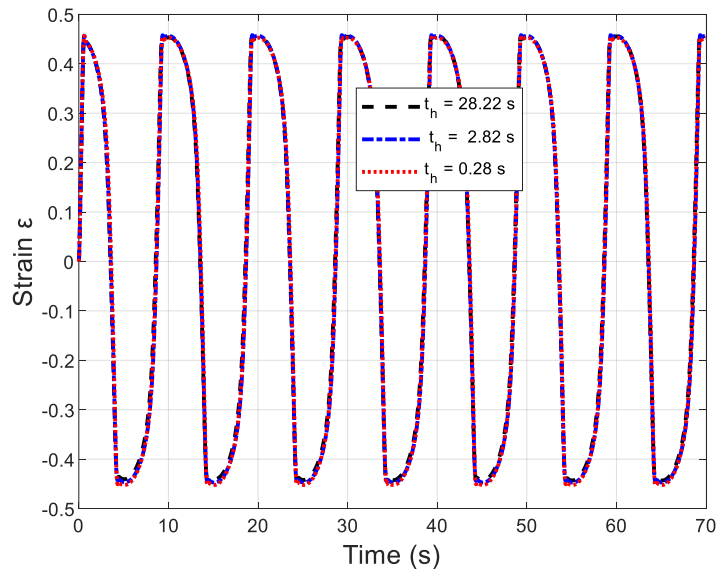
Figure 7. Mechanical response - time curve as a function of heat transfer time

3.3 *Frequency domain analysis*

In this section, the time influence of heat transfer t_h on the frequency responses is analyzed *via* the analytical solution equation (24). Results presented in *Figure 8* shows that, the maximum response amplitude decreases when t_h increases. Furthermore, at $t_h = 0s$, we obtain the FRC in the isothermal case [15] *i.e* the heat exchange is strong between the material and the environment. we note that a given room temperature, at low heat transfer time, the mechanical frequency response curves bend to the right while at high heat transfer time, the mechanical frequency response curves bend to the left. The first bending to the left is due to the softening behaviour in the martensitic phase, while the bending to the right is due to the hardening behaviour in the austenitic phase. These phenomena come from the energy dissipation caused by the heat exchange between the material and the environment, which is reflected in the hysteresis loop of the strain-temperature curves Figure 5. These observations show how much the system responses in SMA depend on both the non-linearity and the condition in which the system exchanges energy with the external environment. Thus, the convective heat exchange in the SMA bar has the effect of damping the vibration response amplitude, which is related to the pseudo-elastic property of SMA. This is why SMA are used as a vibration damper device [42]. While the non-linearity gives it the shape memory effect property. The latter is widely exploited in actuators.
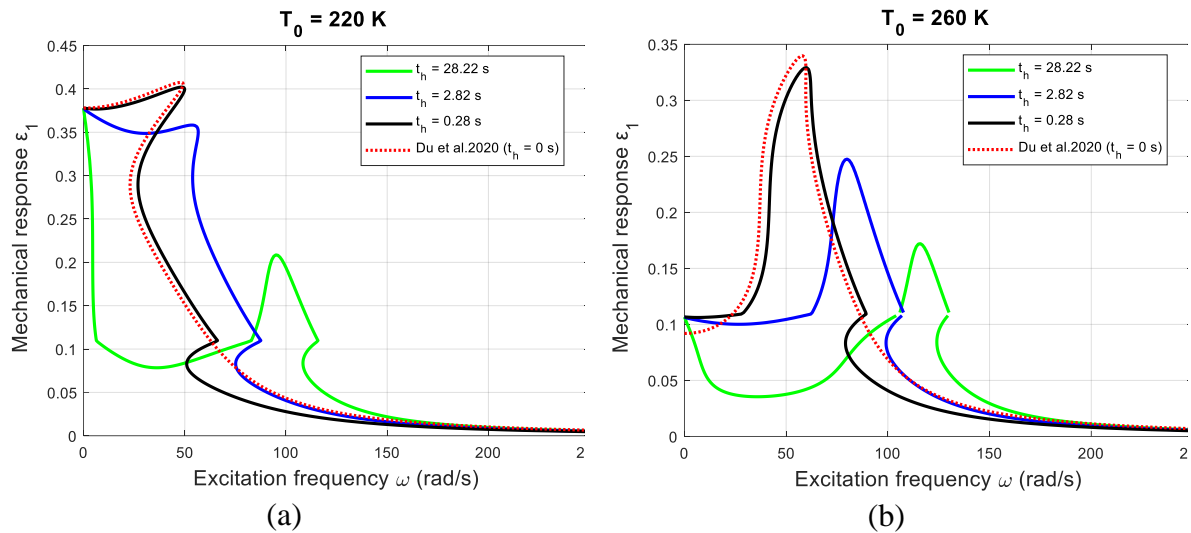
Figure 8. Mechanical frequency response curve as a function of heat transfer time

The *Figure 9* shows the influence of the convective transfer time on the thermal frequency response. It can be seen that when $t_h > 1$s, the thermal response increases and quickly reaches the plateau even at low excitation frequencies, but when time approaches zero, the plateau will be reached at a high excitation frequency (> 250 Hz). It also shows that as the heat transfer time t_h increases, the system reaches the steady state faster. This shows that the state of the system can be controlled by the exchange of heat with the external environment.
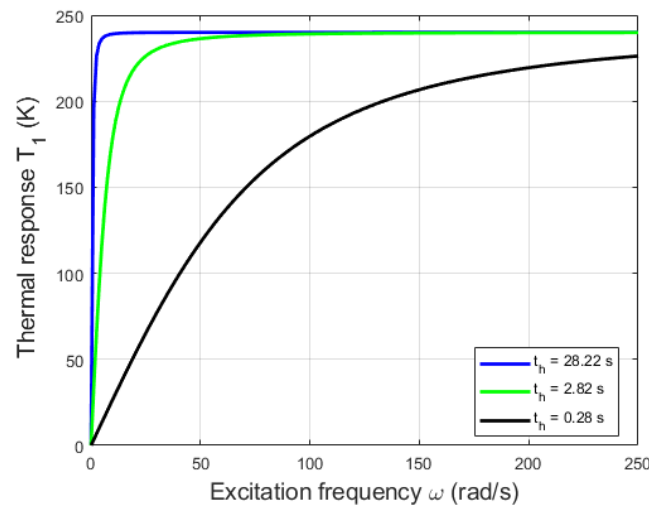
Figure 9. Effect of heat transfer time on thermal frequency responses

These different response-frequency curves show that the dynamic behavior of a system made in SMA can be controlled by heat exchange. The hysteretic behavior of SMA results from the coupling between mechanical (strain) and thermal responses.

4. Conclusion

The objective of this paper was to discuss the non-linear dynamics of the SMA behavior through a mass-bar-damper system taking into account the thermomechanical coupling. A polynomial model has been proposed to describe the force-deformation relationship of the SMA bar, and then the harmonic balance method and the Runge-Kutta method of order fourth are used to obtain responses in the frequency and time domains respectively. The numerical responses of the systems in the frequency and time domains are plotted and the effects of ambient temperature and heat transfer time have been analyzed. It is found that, as the ambient temperature increases, the

resonant frequency gradually increases, while the amplitude decreases. Furthermore, at a given room temperature, at low heat transfer time, the mechanical frequency response curves bend to the right while at high heat transfer time, the mechanical frequency response curves bend to the left. The first bending to the left is due to the softening behaviour in the martensitic phase, while the bending to the right is due to the hardening behaviour in the austenitic phase. These phenomena come from the energy dissipation caused by the heat exchange between the material and the environment, which is reflected in the hysteresis loop of the strain-temperature curves. Finally, the thermal responses can change from a transient state to a stable sinusoidal state in time even under high heat exchange.

Data availability

Data supporting study results are available from the corresponding author upon reasonable request.

Conflict of interest

The author declares no conflict of interest.

References

[1] Abramovich, H.: Intelligent Materials and Structures. De Gruyter (2021)

[2] Khulief, Z.T.: Applications of Shape Memory Alloys. Journal of University of Babylon for Engineering Sciences. 28, 59–72 (2020)

[3] Mabe, J., Calkins, F., Butler, G.: Boeing's variable geometry chevron, morphing aerostructure for jet noise reduction. In: 47th AIAA/ASME/ASCE/AHS/ASC Structures, Structural Dynamics, and Materials Conference 14th AIAA/ASME/AHS Adaptive Structures Conference 7th. p. 2142 (2006)

[4] Jose, S.; Chakraborty, G.; Bhattacharyya, R. Coupled thermo-mechanical analysis of a vibration isolator made of shape memory alloy. *Int. J. Solids Struct.* **2017**, *115-116*, 87–103, https://doi.org/10.1016/j.ijsolstr.2017.03.001.

[5] Jani, J.M., Leary, M., Subic, A., Gibson, M.A.: A review of shape memory alloy research, applications and opportunities. Materials & Design (1980-2015). 56, 1078–1113 (2014)

[6] Morin, C.; Moumni, Z.; Zaki, W. A constitutive model for shape memory alloys accounting for thermomechanical coupling. *Int. J. Plast.* **2011**, *27*, 748–767, https://doi.org/10.1016/j.ijplas.2010.09.005.

[7] O Moussa, M.; Moumni, Z.; Doaré, O.; Touzé, C.; Zaki, W. Non-linear dynamic thermomechanical behaviour of shape memory alloys. *J. Intell. Mater. Syst. Struct.* **2012**, *23*, 1593–1611, https://doi.org/10.1177/1045389x12448446.

[8] Oliveira, H.S.; de Paula, A.S.; Savi, M.A. Dynamical Jumps in a Shape Memory Alloy Oscillator. *Shock. Vib.* **2014**, *2014*, 1–10, https://doi.org/10.1155/2014/656212.

[9] Fremond, M., Miyazaki, S.: Shape Memory Alloys. Springer Vienna, Vienna (1996)

[10] Enemark, S.; Savi, M.; Santos, I. Nonlinear dynamics of a pseudoelastic shape memory alloy system— theory and experiment. *Smart Mater. Struct.* **2014**, *23*, https://doi.org/10.1088/0964-1726/23/8/085018.

[11] Gaikwad, S.R.; Pandey, A.K. Nonlinear Analysis of Shape Memory Devices With Duffing and Quadratic Oscillators. *J. Comput. Nonlinear Dyn.* **2017**, *13*, 011003, https://doi.org/10.1115/1.4037923.

[12] Zhuo, M.; Xia, M.; Sun, Q. Analytical solution of a mass-spring system containing shape memory alloys: Effects of nonlinearity and hysteresis. *Int. J. Solids Struct.* **2019**, *171*, 189–200, https://doi.org/10.1016/j.ijsolstr.2019.04.004.

[13] Rusinek, R.; Rekas, J.; Kecik, K. Vibration Analysis of a Shape Memory Oscillator by Harmonic Balance Method Verified Numerically. *Int. J. Bifurc. Chaos* **2019**, *29*, https://doi.org/10.1142/s0218127419300076.

[14] Weremczuk, A.; Rekas, J.; Rusinek, R. Low- and High-Temperature Primary Resonance in Shape Memory Oscillator Observed by Multiple Time Scales and Harmonic Balance Method. *J. Comput. Nonlinear Dyn.* **2019**, *14*, https://doi.org/10.1115/1.4044312.

[15] Du, H.; He, X.; Wang, L.; Melnik, R. Analysis of shape memory alloy vibrator using harmonic balance method. *Appl. Phys. A* **2020**, *126*, 1–9, https://doi.org/10.1007/s00339-020-03740-x.

[16] Xia, M.; Sun, Q. Jump phenomena of rotational angle and temperature of NiTi wire in nonlinear torsional vibration. *Int. J. Solids Struct.* **2015**, *56-57*, 220–234, https://doi.org/10.1016/j.ijsolstr.2014.11.002.

[17] Zhuo, M. Thermo-mechanical vibration of a hysteretic system with superelastic shape memory alloys. **2015**, https://doi.org/10.14711/thesis-b1450242.

[18] Xia, M.; Sun, Q. Thermomechanical responses of nonlinear torsional vibration with NiTi shape memory alloy – Alternative stable states and their jumps. *J. Mech. Phys. Solids* **2017**, *102*, 257–276, https://doi.org/10.1016/j.jmps.2016.11.015.

[19] Zhuo, M. Timescale competition dictates thermo-mechanical responses of NiTi shape memory alloy bars. *Int. J. Solids Struct.* **2020**, *193-194*, 601–617, https://doi.org/10.1016/j.ijsolstr.2020.02.021.

[20] Yin, H.; He, Y.; Sun, Q. Effect of deformation frequency on temperature and stress oscillations in cyclic phase transition of NiTi shape memory alloy. *J. Mech. Phys. Solids* **2014**, *67*, 100–128, https://doi.org/10.1016/j.jmps.2014.01.013.

[21] Falk, F. Model free energy, mechanics, and thermodynamics of shape memory alloys. *Acta Met.* **1980**, *28*, 1773–1780, https://doi.org/10.1016/0001-6160(80)90030-9.

[22] Olson, G.B., Cohen, M.: Dislocation theory of martensitic transformations. In: Dislocations in solids. pp. 295–407. North-Holland (1986)

[23] Han, Y.; Du, H.; Wang, L.; Melnik, R. A phenomenological model for thermally-induced hysteresis in polycrystalline shape memory alloys with internal loops. *J. Intell. Mater. Syst. Struct.* **2021**, *33*, 1170–1181, https://doi.org/10.1177/1045389x211048228.

[24] Bendame, M. Modeling, simulation, and optimal control of a shape memory alloy actuator. *J. Coupled Syst. Multiscale Dyn.* **2014**, *2*, 126–136, https://doi.org/10.1166/jcsmd.2014.1050.

[25] Savi, M.A., Braga, A.M.B.: Chaotic vibrations of an oscillator with shape memory. Journal of the Brazilian Society of Mechanical Sciences and Engineering. 15, 1–20 (1993)

[26] Wang, L.; Melnik, R.V. Nonlinear dynamics of shape memory alloy oscillators in tuning structural vibration frequencies. *Mechatronics* **2012**, *22*, 1085–1096, https://doi.org/10.1016/j.mechatronics.2012.09.004.

[27] Abeyaratne, R.; Knowles, J.K. On a shock-induced martensitic phase transition. *J. Appl. Phys.* **2000**, *87*, 1123–1134, https://doi.org/10.1063/1.371989.

[28] Wilde, K.; Gardoni, P.; Fujino, Y. Base isolation system with shape memory alloy device for elevated highway bridges. *Eng. Struct.* **2000**, *22*, 222–229, https://doi.org/10.1016/s0141-0296(98)00097-2.

[29] Jose, S.; Chakraborty, G.; Bhattacharyya, R. Force transmissibility characteristics of a pseudoelastic oscillator. *J. Intell. Mater. Syst. Struct.* **2019**, *31*, 349–363, https://doi.org/10.1177/1045389x19888736.

[30] Cotta, R.M., Mikhailov, M.D.: Heat Conduction: Lumped Analysis, Integral Transforms, Symbolic Computation, first ed. John Wiley & Sons, New Jersey. (1997)

[31] Yin, H. Oscillations of thermal and mechanical fields during cyclic phase transition. **2014**, https://doi.org/10.14711/thesis-b1251149.

[32] He, Y.J.; Sun, Q.P. Frequency-dependent temperature evolution in NiTi shape memory alloy under cyclic loading. *Smart Mater. Struct.* **2010**, *19*, https://doi.org/10.1088/0964-1726/19/11/115014.

[33] Yan, Y.; Yin, H.; Sun, Q.P.; Huo, Y. Rate dependence of temperature fields and energy dissipations in non-static pseudoelasticity. *Contin. Mech. Thermodyn.* **2012**, *24*, 675–695, https://doi.org/10.1007/s00161-012-0254-9.

[34] Ghorbel, A.; Zghal, B.; Abdennadher, M.; Walha, L.; Haddar, M. Analysis of Strongly Nonlinear Systems by Using HBM-AFT Method and Its Comparison with the Five-Order Runge–Kutta Method: Application to Duffing Oscillator and Disc Brake Model. *Int. J. Appl. Comput. Math.* **2020**, *6*, 1–20, https://doi.org/10.1007/s40819-020-0803-z.

[35] Yang, J.; Xiong, Y.; Xing, J. Nonlinear power flow analysis of the Duffing oscillator. *Mech. Syst. Signal Process.* **2013**, *45*, 563–578, https://doi.org/10.1016/j.ymssp.2013.11.004.

[36] Qu, R.; Li, S.; Bi, Q. Forced vibration of shape memory alloy spring oscillator and the mechanism of sliding bifurcation with dry friction. *Adv. Mech. Eng.* **2019**, *11*, https://doi.org/10.1177/1687814019851976.

[37] Mosley, M.J.; Mavroidis, C. Experimental Nonlinear Dynamics of a Shape Memory Alloy Wire Bundle Actuator. *J. Dyn. Syst. Meas. Control.* **1999**, *123*, 103–112, https://doi.org/10.1115/1.1344243.

[38] Hartl, D.J.; Lagoudas, D. Aerospace applications of shape memory alloys. *Proc. Inst. Mech. Eng. Part G: J. Aerosp. Eng.* **2007**, *221*, 535–552, https://doi.org/10.1243/09544100jaero211.

[39] Romano, R.; Tannuri, E.A. Modeling, control and experimental validation of a novel actuator based on shape memory alloys. *Mechatronics* **2009**, *19*, 1169–1177, https://doi.org/10.1016/j.mechatronics.2009.03.007.

[40] Maletta, C.; Falvo, A.; Furgiuele, F. A Phenomenological Approach for Real-Time Simulation of the Two-Way Shape Memory Effect in NiTi Alloys. *J. Eng. Mater. Technol.* **2007**, *130*, 011003, https://doi.org/10.1115/1.2806264.

[41] Helbert, G.; Saint-Sulpice, L.; Chirani, S.A.; Dieng, L.; Lecompte, T.; Calloch, S.; Pilvin, P. Experimental characterisation of three-phase NiTi wires under tension. *Mech. Mater.* **2014**, *79*, 85–101, https://doi.org/10.1016/j.mechmat.2014.07.020.

[42] Dieng, L.; Helbert, G.; Chirani, S.A.; Lecompte, T.; Pilvin, P. Use of Shape Memory Alloys damper device to mitigate vibration amplitudes of bridge cables. *Eng. Struct.* **2013**, *56*, 1547–1556, https://doi.org/10.1016/j.engstruct.2013.07.018.